Developmental Cell
Article

# TPP1 Is Required for TERT Recruitment, Telomere Elongation during Nuclear Reprogramming, and Normal Skin Development in Mice

Agueda M. Tejera,[1,4] Martina Stagno d'Alcontres,[1,4] Maria Thanasoula,[2] Rosa M. Marion,[1] Paula Martinez,[1] Chunyan Liao,[2] Juana M. Flores,[3] Madalena Tarsounas,[2] and Maria A. Blasco[1,*]
[1]Telomeres and Telomerase Group, Molecular Oncology Program, Spanish National Cancer Centre (CNIO), Melchor Fernández Almagro 3, Madrid E-28029, Spain
[2]Telomere and Genome Stability Group, The CR-UK/MRC Gray Institute for Radiation Oncology and Biology, Old Campus Road, Oxford OX3 7DQ, UK
[3]Animal Surgery and Medicine Department, Facultad de Veterinaria, Universidad Complutense de Madrid, 28029 Madrid, Spain
[4]These authors contributed equally to this work
*Correspondence: mblasco@cnio.es
DOI 10.1016/j.devcel.2010.03.011

## SUMMARY

**The TPP1/ACD protein (hereafter TPP1) is a component of the shelterin complex at mammalian telomeres. Here we find that *Tpp1*-deficient mouse embryonic fibroblasts (MEFs) show increased chromosomal instability including sister chromatid fusions and chromosomes with multitelomeric signals related to telomere fragility. *Tpp1* deletion decreases both TERT (the telomerase catalytic subunit) binding to telomeres in MEFs and telomerase function at chromosome ends in vivo. Abrogation of *Tpp1* abolished net telomere elongation in the context of nuclear reprogramming of MEFs into induced pluripotent stem cells, whereas *Tpp1* deletion in stratified epithelia of *Tpp1*$^{\Delta/\Delta}$*K5-Cre* mice resulted in perinatal death, severe skin hyperpigmentation, and impaired hair follicle morphogenesis. p53 deficiency rescues skin hyperpigmentation and hair growth in these mice, indicating that p53 restricts proliferation of *Tpp1*-deficient cells. These results suggest a telomere-capping model where TPP1 protects telomere integrity and regulates telomerase recruitment to telomeres, thereby preventing early occurrence of degenerative pathologies.**

## INTRODUCTION

The TPP1/ACD protein (hereafter TPP1) is part of the shelterin complex bound to mammalian telomeres, encompassing TRF1, TRF2, POT1a/b, TPP1, TIN2, and RAP1 in the mouse (de Lange, 2005; Liu et al., 2004). Evidence from *Schizosaccharomyces pombe* and mammals suggests that TPP1 interacts with POT1 and that this interaction is important for telomerase regulation at chromosome ends and for bridging TRF1 and TRF2 complexes at the double-stranded telomeric repeats (Miyoshi et al., 2008; Xin et al., 2007). In addition, TPP1 is required for POT1 binding and protection of telomeres (Hockemeyer et al., 2007).

A spontaneous recessive mutation in a splice donor site of the *Tpp1* gene is responsible for the *acd* mouse, a hypomorphic mouse model with decreased TPP1 levels (Keegan et al., 2005). These mice can survive to adulthood but show developmental defects including adrenocortical dysplasia and hypofunction, skin hyperpigmentation, and infertility (Keegan et al., 2005), as well as increased incidence of cancer in a *p53* null background (Else et al., 2009). Cells derived from *acd* mice show increased telomere damage and telomere fusions but a normal telomere length (Else et al., 2007; Hockemeyer et al., 2007). A further understanding of the role of TPP1 in telomere regulation in vivo and in mouse development and disease has been missing to date due to lack of mouse models with complete TPP1 abrogation.

Here we generated *Tpp1*-deficient mouse embryonic fibroblasts (MEFs) as well as mice with targeted *Tpp1* deletion to the stratified epithelia. Both MEFs and mice deleted for *Tpp1* show induction of telomere damage foci (TIFs) and cell-cycle arrest, demonstrating that TPP1 protects telomeres from eliciting a DNA damage response (DDR). *Tpp1* null mice die perinatally and show severe skin hyperpigmentation and defective hair follicle morphogenesis. These phenotypes are rescued by p53 abrogation, indicating that p53 is a main effector of proliferative defects associated with *Tpp1* deletion. *Tpp1* null cells also show increased sister telomere fusions and chromosome ends with more than one telomeric signal (multitelomeric signals; MTS), recently related to telomere fragility (Martinez et al., 2009; Sfeir et al., 2009).

Interestingly, *Tpp1* deletion resulted in decreased TERT (the telomerase catalytic subunit) binding to telomeres and accelerated telomere shortening both in MEFs and mice. Moreover, *Tpp1* null cells fail to elongate their telomeres when reprogrammed into pluripotent stem cells by using defined factors, the so-called induced pluripotent stem (iPS) cells (Takahashi and Yamanaka, 2006), a process that is dependent on telomerase activity (Marion et al., 2009a, 2009b), thus indicating that TPP1 is essential for telomere elongation in vivo. Together, these results suggest a telomere-capping model where TPP1 not only

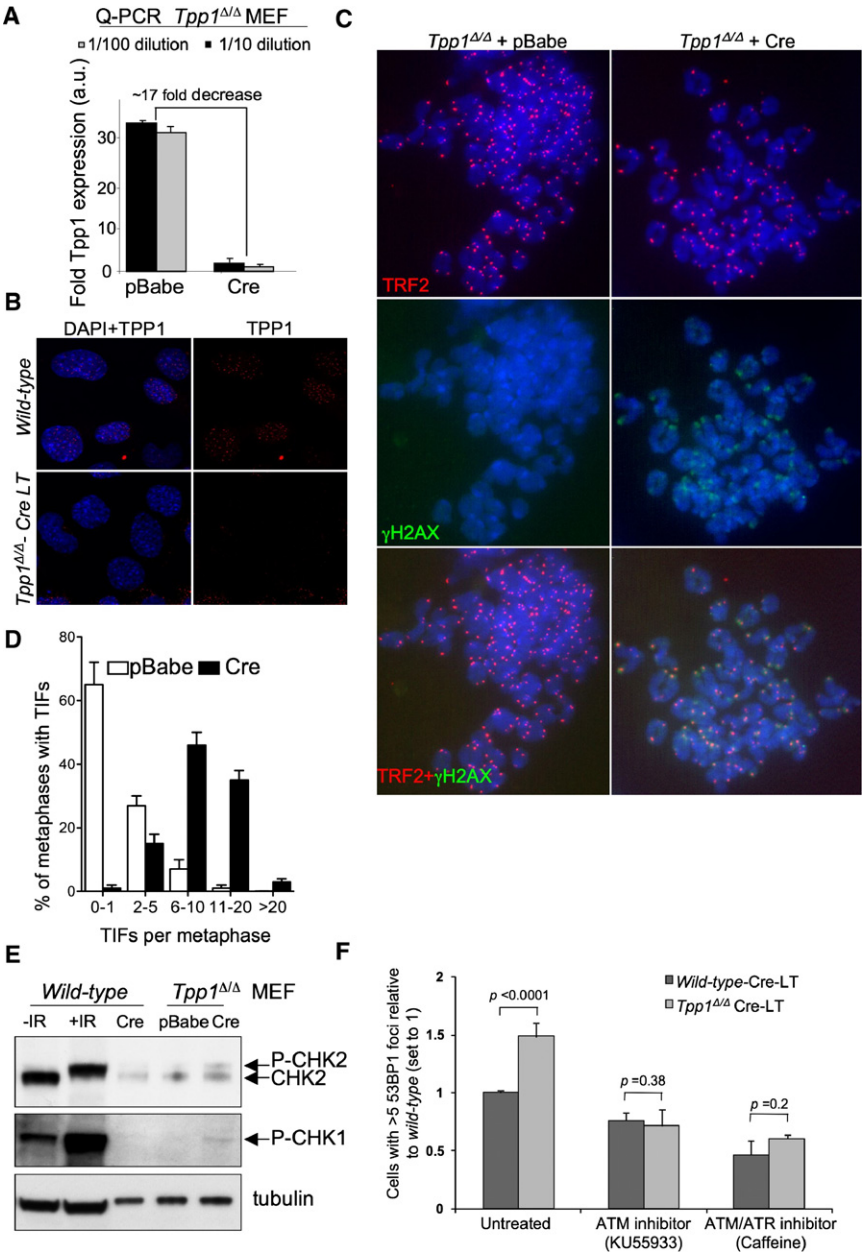


**Figure 1. DDR Activation in *Tpp1*-Deleted MEFs**

(A) Quantification of *Tpp1* mRNA levels by Q-PCR in $Tpp1^{\Delta/\Delta}$-Cre-LT MEFs versus control cells infected with pBabe vector.

(B) Immunofluorescence detection of mouse TPP1 (red) in the indicated MEFs. DNA was counterstained with DAPI (blue).

(C) Immunofluorescence detection of γH2AX (green) combined with TRF2 staining of the telomeres (red) in the indicated MEFs.

(D) The percentage of metaphase nuclei exhibiting the indicated number of TIFs per metaphase was determined for at least 50 metaphases per genotype prepared as in (C).

(E) Western blot detection of phospho-CHK1 and -CHK2 in the indicated MEFs treated with Hit&Run Cre vector. Wild-type MEFs treated with 0 or 10 Gy of ionizing radiation served as a control for checkpoint activation. Tubulin was used as a loading control.

(F) Rescue of 53BP1 DNA damage foci in *Tpp1*-depleted MEFs treated with 10 μM KU55933 (an ATM inhibitor) or 5 μM caffeine (dual ATM/ATR inhibitor). Two independent experiments were performed in duplicate, and at least 100 cells were analyzed per condition in each experiment. The data represent mean values relative to wild-type ± standard error. Statistical significance was determined by Student's t test.

prevents the induction of a DDR at telomeres by preventing fusions and telomere breakage but is also required for telomere elongation by telomerase.

## RESULTS

### *Tpp1*-Deficient MEFs Undergo Rapid Proliferative Arrest Concomitant with DDR Activation at Chromosome Ends

We first established MEFs from wild-type and conditional $Tpp1^{flox/flox}$ mice and infected them with a pBabe-Cre retrovirus ($Tpp1^{\Delta/\Delta}$-Cre MEFs), which resulted in undetectable *Tpp1* mRNA levels by quantitative PCR (Q-PCR) and lack of TPP1 protein by immunofluorescence staining (Figures 1A and 1B; see Supplemental Experimental Procedures available online). As *Tpp1*-deficient MEFs failed to proliferate in vitro, we downregulated the expression of p53 by using a small hairpin RNA (shRNA) against p53 and generated $Tpp1^{\Delta/\Delta}$-Cre-shp53 MEFs, or alternatively suppressed both the p53 and Rb pathways by SV40 large T (LT) antigen expression in $Tpp1^{\Delta/\Delta}$-Cre-LT MEFs (Figures S1A–S1C). In both cases, we observed a significant rescue of cell proliferation compared to $Tpp1^{\Delta/\Delta}$-Cre MEFs (not shown and Figure S1C for $Tpp1^{\Delta/\Delta}$-Cre-shp53 MEFs). These findings indicate *Tpp1* deletion results in rapid cell-cycle arrest which is mediated by the p53 and pRB pathways.

To determine whether proliferation defects of *Tpp1*-deleted MEFs are mediated by checkpoint responses induced by telomere dysfunction, we next addressed whether *Tpp1* abrogation leads to telomere damage. γH2AX foci mark the presence of critically short/dysfunctional telomeres or TIFs (d'Adda di Fagagna et al., 2003; Takai et al., 2003). After transient expression of the Cre recombinase from the self-inactivating Hit&Run retrovirus (Silver and Livingston, 2001), most $Tpp1^{\Delta/\Delta}$ cells showed γH2AX foci at telomeres of spread mitotic chromosomes (Figure 1C), reaching 6–20 TIFs per metaphase (Figure 1D). TIF induction following *Tpp1* deletion was accompanied by phosphorylation of the CHK1 and CHK2 checkpoint kinases (Figure 1E), whereas this was not observed in wild-type controls. As a positive control, wild-type MEFs exposed to 10 Gy of

ionizing radiation showed a complete shift of the CHK2 lower band and a robust CHK1 phosphorylation. To dissect the relative importance of ATM and ATR pathways in the DDR induced by *Tpp1* deficiency, we determined 53BP1 DNA damage foci upon inhibition of ATM (KU55933 inhibitor; Hickson et al., 2004) or both ATM/ATR kinases (caffeine). As shown in Figure 1F, 53BP1 DNA damage foci induced by *Tpp1* abrogation were rescued when either ATM or both ATM and ATR were inhibited, indicating that both DNA damage signaling pathways are activated upon *Tpp1* deletion.

### *Tpp1*$^{\Delta/\Delta}$*K5-Cre* Mice Show Increased Telomere Damage and G2/M Mitotic Arrest in the Epidermis

To study the impact of *Tpp1* abrogation in the context of the organism, we targeted deletion of *Tpp1* to mouse stratified epithelia. For this, we crossed conditional *Tpp1*$^{flox/flox}$ mice or *Tpp1*$^{+/flox}$ mice with *K5-Cre* mice that constitutively express the Cre recombinase under the control of the keratin 5 (K5) promoter from day 11.5 of embryonic development onward (Ramirez et al., 1994), thereby generating *Tpp1*$^{\Delta/\Delta}$*K5-Cre* mice (Figures 2A and 2B). *Tpp1*$^{\Delta/\Delta}$*K5-Cre* mice show complete excision of *Tpp1* exon 1 in the epidermis whereas no deletion can be detected in the dermis (Figure 2B), in agreement with K5 expression pattern (Ramirez et al., 1994). Accordingly, *Tpp1* expression was abrogated in *Tpp1*$^{\Delta/\Delta}$*K5-Cre* epidermis, as determined both by Q-PCR on skin keratinocytes (Figure 2C) and TPP1 immunofluorescence on skin sections (Figure 2D).

In analogy to *Tpp1*-deficient MEFs, *Tpp1*$^{\Delta/\Delta}$*K5-Cre* epidermis showed increased γH2AX-positive cells compared to wild-type mice (Figures 2E and 2F), and these γH2AX foci colocalized with telomeres (TRF1/γH2AX colocalization) in a high percentage of cells (Figures 2E and 2F), indicative of persistent DDR activation at telomeres in *Tpp1*-deleted mouse epidermis.

Finally, in analogy to severe cell-cycle arrest in *Tpp1*-deleted MEFs, flow cytometry analysis of freshly isolated, noncultured skin keratinocytes showed that a significant percentage of *Tpp1*$^{\Delta/\Delta}$*K5-Cre* keratinocytes was arrested in G2/M with a 4n DNA content, indicating failure to undergo mitosis upon *Tpp1* deletion (Figures 2G and 2H). Furthermore, *Tpp1*-deleted keratinocytes showed increased polyploidy as indicated by the presence of >4n populations (Figures 2G and 2H). Together, these results indicate that *Tpp1* deletion in the context of the mouse epidermis leads to a persistent telomere-originated DDR which is accompanied by G2/M arrest and increased polyploidy.

### TPP1 Prevents Sister Telomere Fusions and Telomere Fragility

To address a role for TPP1 in telomere protection, we performed metaphase fluorescence in situ hybridization (FISH) staining with a telomeric probe on *Tpp1* null, LT-immortalized MEFs. *Tpp1*$^{\Delta/\Delta}$-Cre-LT MEFs showed significantly increased frequencies of sister telomere fusions compared to *Tpp1*$^{+/+}$-Cre-LT controls (Figures 3A–3C). *Tpp1*-deleted MEFs also showed a significant increase in chromosome ends with MTS (2–4 per metaphase; Figures 3A–3C), recently related to increased telomere fragility (Blanco et al., 2007; Martinez et al., 2009; Munoz et al., 2005; Sfeir et al., 2009). In agreement with this, MTS were increased in wild-type MEFs treated with aphidicolin, known to induce replication fork stalling and breakage at fragile sites (Durkin and Glover, 2007; Sfeir et al., 2009), and further increased in similarly treated *Tpp1*-deficient MEFs (Figure 3C), suggesting that telomeres lacking TPP1 are prone to breakage. Accordingly, breaks and fragments but not telomere fusions were increased in aphidicolin-treated wild-type and *Tpp1* null MEFs (Figure 3C). Replication fork stalling results in fork fragmentation and resection, leading to accumulation of ssDNA. Supporting aberrant replication and breakage of TPP1-depleted telomeres, we observed an increased colocalization of the replication factor PCNA and of ssDNA (as indicated by BrdU incorporation) with telomeres (as visualized by TRF1 immunofluorescence) compared with wild-type cells (Figures 3D–3I). As a positive control, BrdU staining was increased in γ-irradiated *Tpp1*-depleted cells (Figure 3G). Together, these data indicate that TPP1 deletion induces telomere uncapping leading to sister telomere fusions, as well as increased telomere fragility and breakage resulting in MTS. Finally, as these defects are similar, although milder, to those induced by TRF1 deletion in MEFs (Martinez et al., 2009), we ruled out defective TRF1 expression in these cells as indicated by TRF1 immunofluorescence (Figure S2).

### TPP1 Is Required for TERT Binding to Telomeres and Telomere Maintenance In Vivo

DDR activation at chromosome ends also occurs in cells deficient for other shelterin components, including POT1, TRF2, and TRF1 (Celli and de Lange, 2005; Hockemeyer et al., 2006; Martinez et al., 2009; Sfeir et al., 2009; Wu et al., 2006). As TPP1 is already known to mediate POT1 binding to telomeres (Hockemeyer et al., 2007), here we set out to address whether binding of TRF1, TRF2, and RAP1 was affected by TPP1 deletion (Figures 4A–4D). In chromatin fractionation assays, binding of TRF1, TRF2, and RAP1 to chromatin was similar in wild-type and *Tpp1*-deficient MEFs (Figures 4A and 4B). Chromatin immunoprecipitation (ChIP) assays also indicated normal binding of TRF1 and TRF2 to telomeres in the absence of TPP1 binding (Figures 4C and 4D). In analogy with MEF results, *Tpp1*-deleted epidermis showed normal TRF1 immunofluorescence (Figure 4E).

Based on its direct interaction with telomerase (Xin et al., 2007), TPP1 has been proposed to regulate telomerase at chromosome ends. Here we set out to address whether TPP1 is required for TERT binding to telomeres in vivo. As shown in Figures 4A and 4F, *Tpp1*-deficient MEFs showed decreased TERT binding to chromatin in the presence of normal binding of H3 and the other shelterin components. As controls, we performed chromatin fractionation of MEFs deficient in either of the telomerase core components TERT (*Tert*$^{-/-}$) and *Terc* (*Terc*$^{-/-}$) (Blasco et al., 1997; Liu et al., 2000). *Tert*$^{-/-}$ MEFs did not show detectable TERT binding to chromatin, confirming the specificity of the TERT antibodies used (Figure 4F) (Experimental Procedures). *Terc*$^{-/-}$ MEFs showed normal TERT binding to chromatin (Figure 4F), which is also dependent on TPP1 (Figures S3A and S3B), as indicated by using a small hairpin RNA against Tpp1 (shTpp1) (Experimental Procedures). We extended these findings to HeLa cells, where *Tpp1* knockdown also resulted in decreased TERT binding to chromatin (Figure S3C). Importantly, by using telomeric ChIP assays, we further demonstrate defective TERT binding specifically to

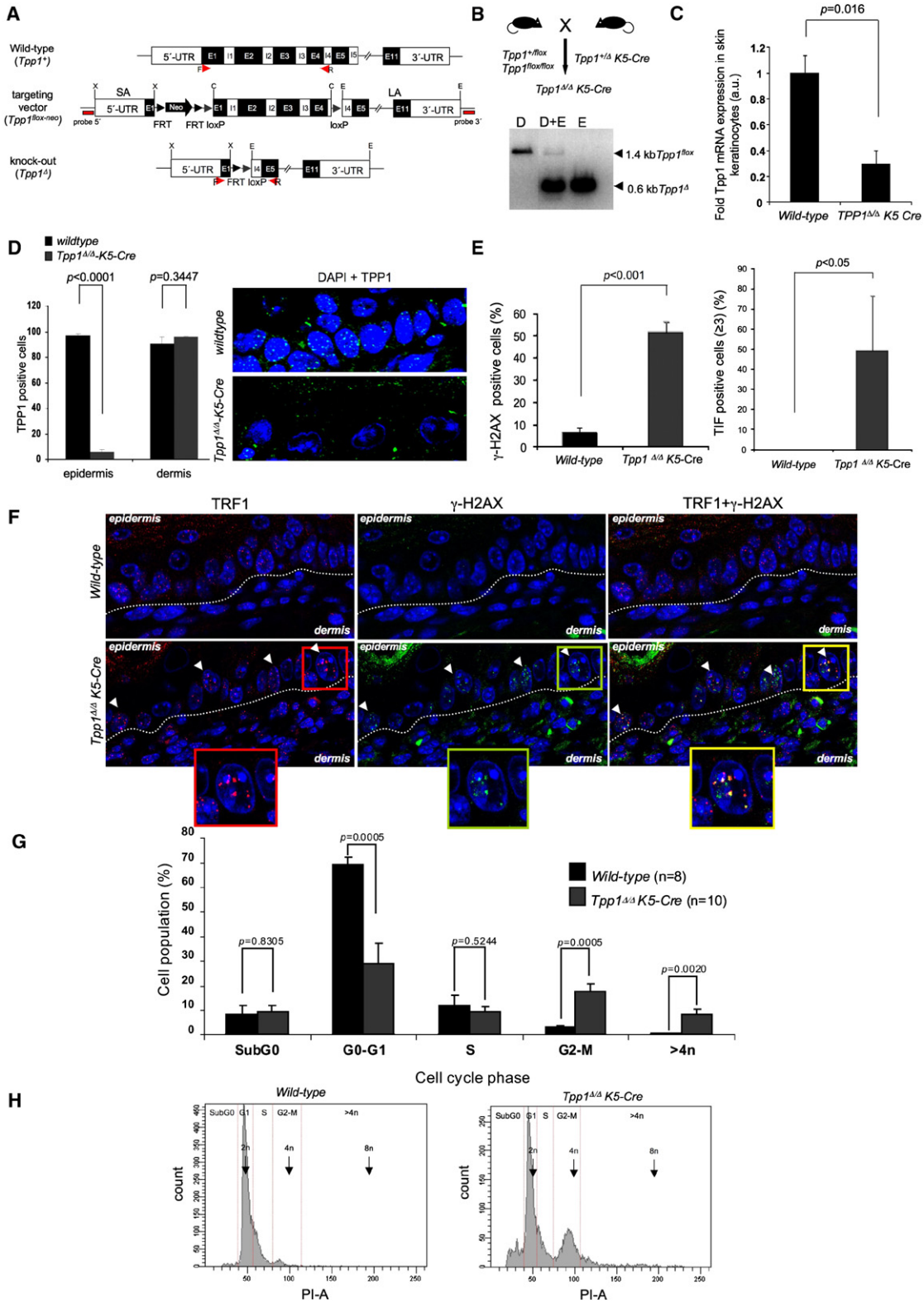


**Figure 2. *Tpp1* Deficiency Leads to Induction of TIFs and G2/M Mitotic Arrest in Mouse Epidermis**

(A) Schematic outline of wild-type (*Tpp1*$^{+}$), floxed (*Tpp1*$^{flox\text{-}neo}$), and deleted (*Tpp1*$^{-\Delta}$) loci.

(B) Breeding strategy to generate *Tpp1*$^{\Delta/\Delta}$*K5-Cre* mice and demonstration that *Tpp1* deletion is specifically targeted to the epidermis. PCR amplification of *Tpp1* alleles in whole skin (dermis + epidermis; D+E), dermis (D), and epidermis (E) of *Tpp1*$^{\Delta/\Delta}$*K5-Cre* mice using the F and R primers (Experimental Procedures).

telomeric repeats in the absence of TPP1 (Figures 4G and 4H). Absence of TERT binding was not due to decreased TERT mRNA expression in *Tpp1* null cells (Figure S3D), in agreement with normal telomerase TRAP (telomere repeat amplification protocol) activity in these cells (Figure S3D). Together, these results identify TPP1 as a telomerase recruitment factor in vivo.

We next addressed the impact of *Tpp1* deficiency on telomere length maintenance by performing telomere quantitative FISH (Q-FISH) analysis on MEF metaphases. Proliferating $Tpp1^{\Delta/\Delta}$-Cre-shp53 and $Tpp1^{\Delta/\Delta}$-Cre-LT MEFs showed decreased telomere fluorescence when compared to their corresponding wild-type controls (Figure 5A), suggesting a faster rate of telomere shortening in the absence of TPP1. Importantly, this shortening was not accompanied by changes in the G-strand overhang (Figure S4). Finally, we confirmed an accelerated rate of telomere shortening in $Tpp1^{\Delta/\Delta}$*K5-Cre* epidermis compared to wild-type skin both by using telomere Q-FISH following correction by centromeric fluorescence (Figure 5B) and by terminal restriction fragment (TRF) analysis (Figure 5C), a Southern-based technique that estimates the size of telomere-containing terminal fragments (Experimental Procedures).

## TPP1 Is Required for Net Telomere Elongation during Nuclear Reprogramming

The results described above suggest a role for TPP1 in TERT recruitment to telomeres and telomere maintenance, but they do not address whether TPP1 is required for telomere elongation by telomerase. To this end, we took advantage of the recently described process of generation of iPS cells from parental differentiated cells (Takahashi and Yamanaka, 2006). In particular, during iPS cell generation, telomeres undergo a net elongation compared to the parental MEFs, a process which is dependent on telomerase activity (Marion et al., 2009a, 2009b). Here we generated iPS cell clones from wild-type and *Tpp1* null MEFs simultaneously knocked down for p53 by using a small hairpin RNA against p53 (shp53), which allows efficient reprogramming of parental cells with dysfunctional telomeres (Marion et al., 2009a) (Figures 5D–5F). Four independent wild-type Cre-shp53 iPS clones showed a net telomere elongation of approximately 10 kb at passage 2-3 after clone isolation compared to parental MEFs (Figures 5D and 5E). In marked contrast, none of the four *Tpp1* null iPS clones studied showed detectable telomere elongation compared to the parental MEFs; instead, a modest telomere shortening was observed (Figures 5D and 5E). As *Tpp1* null cells have normal telomerase activity in vitro (see Figure S3D), these results indicate that TPP1 is necessary for telomerase-mediated telomere elongation in vivo. As a control for pluripotency, a similarly high expression of the endogenous pluripotency genes Oct4 and Nanog was detected in both wild-type and *Tpp1* null iPS clones compared to a lack of expression in the parental MEFs (Figure 5F).

## *Tpp1*-Conditional Deletion in Stratified Epithelia Leads to Perinatal Death, Skin Hyperpigmentation, and Severe Defects in Hair Follicle Morphogenesis

In contrast to *acd* mice that can survive to adulthood, $Tpp1^{\Delta/\Delta}$*K5-Cre* mice showed a fully penetrant perinatal mortality with no mice surviving more than 2 weeks (Figure 6A; see also Figure 7D). In addition, $Tpp1^{\Delta/\Delta}$*K5-Cre* mice did not gain weight in the days following birth (Figure 6B; see also Figure 7E) due to epithelial abnormalities in the oral mucosa (Table S1; Figure S5A) which prevented feeding. At birth, $Tpp1^{\Delta/\Delta}$*K5-Cre* mice show severe skin hyperpigmentation, which is aggravated the following days concomitant with severe skin scaling and dryness (compare day 4 and day 7; Figure 6C). Histopathological analysis of $Tpp1^{\Delta/\Delta}$*K5-Cre* epidermis revealed lack of mature hair follicles and sebaceous glands (Figures 6D–6J; Figure S5), as well as an abnormally high expression of cytokeratin 6 compared to wild-type epidermis (Figure 6D), a pathological condition associated with skin diseases such as psoriasis and skin cancer (Stoler et al., 1989). Cytokeratins 10 and 14, which mark suprabasal and basal skin layers, respectively, showed a normal expression pattern (Figure 6D), suggesting that *Tpp1* deficiency does not affect skin differentiation. Concomitantly with degenerative lesions, all $Tpp1^{\Delta/\Delta}$*K5-Cre* mice presented areas of focal dysplasia in the skin (Table S1; Figure S5A) which were also present in other stratified epithelia (Table S1; Figure S5A). Severe skin abnormalities in $Tpp1^{\Delta/\Delta}$*K5-Cre* mice were accompanied by a defective epithelial barrier function (Figure 6E), which together with the lack of nourishment may contribute to their fully penetrant perinatal mortality (McGavin and Zachary, 2007).

## Severe Hair Morphogenesis Defects in $Tpp1^{\Delta/\Delta}$*K5-Cre* Epidermis

Lack of mature hair follicles and sebaceous glands in $Tpp1^{\Delta/\Delta}$*K5-Cre* skin suggests a defect in the hair bulge stem cell (SC) compartment (Flores et al., 2005; Martinez et al., 2009; Stout and Blasco, 2009). Here we set out to examine the impact of *Tpp1* abrogation on hair follicle morphogenesis by studying the expression of the Sox9 gene, which marks hair bulge SC

(C) *Tpp1* mRNA levels as determined by Q-PCR in three neonate keratinocytes per genotype. Actin was used to normalize samples. Error bars represent standard error. Student's t test was used for statistical analysis, and the p value is indicated.
(D) Quantification of TPP1-positive cells in epidermis and dermis of three or four independent wild-type and $Tpp1^{\Delta/\Delta}$*K5-Cre* newborn mice. The percentage of positive cells per genotype is shown. Error bars represent standard error. Student's t test was used for statistical analysis and p values are indicated. Right: representative images of immunofluorescence staining in epidermis using a TPP1 antibody (green). Nuclei are counterstained with DAPI (blue).
(E) Percentage of skin basal-layer keratinocytes showing γ-H2AX foci (left), and percentage of these cells displaying γ-H2AX colocalization with telomeres (TRF1) in back skin sections of mice of the indicated genotypes. At least 300 cells from three independent mice were scored per genotype. Error bars represent standard error. Student's t test was used for statistical analysis, and p values are indicated.
(F) Representative images of TRF1 (red) and γ-H2AX (green) fluorescence, and the combined images. Colocalization events (white arrows) are detected by yellow fluorescence. The dotted line separates epidermis from dermis.
(G) Cell-cycle analysis of primary keratinocytes from wild-type and $Tpp1^{\Delta/\Delta}$*K5-Cre* neonates. Quantification of the percentage of cells at different phases of the cell cycle by FACS is represented. Cells were stained with propidium iodide (PI-A). n, independent newborn mice used per genotype. Error bars represent standard error. The Student's t test was used for statistical analysis, and p values are indicated.
(H) Representative examples of the FACS histograms.

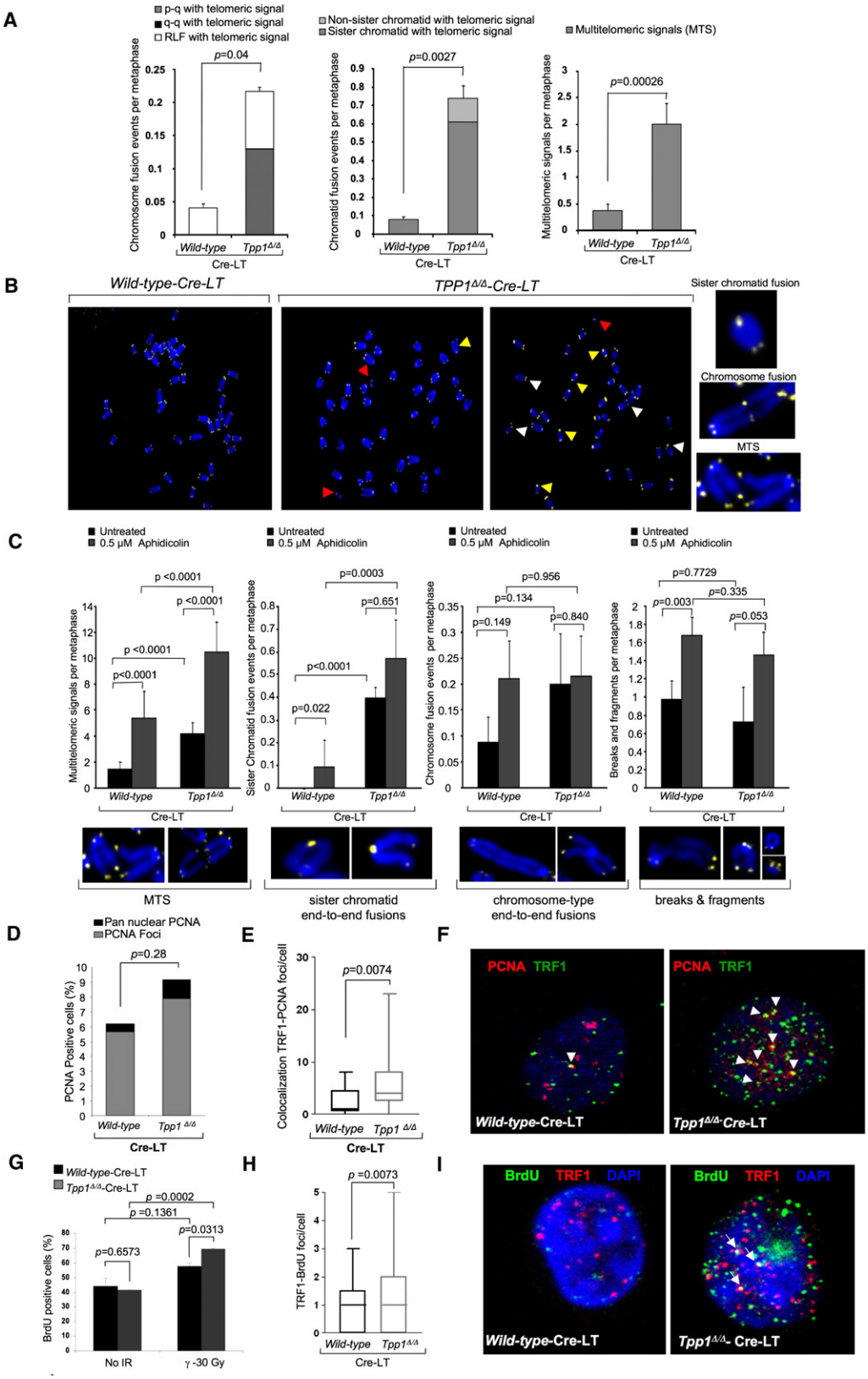


**Figure 3. Increased Sister Telomere Fusions and Telomere Fragility in *Tpp1*-Deficient MEFs**

(A) Frequency of aberrations in metaphase spreads from the indicated genotypes and conditions. At least 20 metaphases from two independent MEFs per genotype were analyzed. Error bars represent standard error. Statistical comparisons using the $\chi^2$ test are shown and p values are indicated.

precursors during embryonic and early postnatal development (Nowak et al., 2008; Vidal et al., 2005). Wild-type epidermis showed intense Sox9 expression at the hair bulge SC niche at P4, whereas it was almost undetectable at the interfollicular epidermis at this stage (Figure 6F). In contrast, age-matched *Tpp1*-deficient epidermis showed reduced Sox9 expression at the base of the hair primordiums whereas it was elevated in the interfollicular epidermis (Figure 6F), indicative of lack of mature hair bulge formation in *Tpp1*$^{\Delta/\Delta}$*K5-Cre* skin. We also failed to detect expression of the hair bulge marker K15 in *Tpp1*$^{\Delta/\Delta}$*K5-Cre* hair primordiums, whereas it was readily detected at the hair bulge in age-matched wild-type hair follicles (Liu et al., 2003) (Figure 6G).

A number of molecular signals are involved in instructing epithelial cells to adopt a hair follicle fate and to establish and maintain functional mature hair follicles (reviewed in Blanpain and Fuchs, 2009). Wnt/β-catenin signaling is the earliest molecular signal known to determine hair follicle development (Huelsken et al., 2001; Paus et al., 1999; Zhang et al., 2008). Interestingly, we observed no significant differences in nuclear β-catenin staining at E16.5–E17.5 placodes and hair pegs (Figure S5B) between wild-type and *Tpp1* null mice, suggesting that β-catenin nuclear signaling is not altered by *Tpp1* abrogation and, therefore, is not likely to be causative of hair growth defects in these mice. Also in agreement with normal β-catenin expression, we observed no differences in the number of E17.5 placodes/hair pegs (Figure S5C) and P2 developing hair follicles (Figure 6H). We next studied the ability of developing hair follicles to downgrow into the dermis by using a dermal papilla staining (Experimental Procedures). We observed a dramatic defect in hair follicle downgrowth in *Tpp1* null epidermis, as indicated by dermal papilla staining restricted to the epidermis in P1 *Tpp1* null epidermis in contrast to 100% internalization of the dermal papilla in age-matched wild-type epidermis (stage 1 versus stages 3–5 in wild-type skin; Huelsken et al., 2001; Paus et al., 1999) (see Figure 6I). At this stage, we also failed to detect expression of the GATA-3 differentiation marker, which is normally expressed at the inner root sheath in wild-type follicles (white arrows; Figure S5D) (Kaufman et al., 2003). Next, we studied whether downstream signals of Wnt known to be involved in hair follicle downgrowth and morphogenesis, such as Sonic hedgehog (Shh), are altered in *Tpp1* null skin (Huelsken et al., 2001; St-Jacques et al., 1998). However, *Shh* mRNA expression was similar at hair pegs of wild-type and *Tpp1*$^{\Delta/\Delta}$*K5-Cre* E17.5 embryos (Figure S5E), arguing that abnormal *Shh* expression is not responsible for defective formation of mature hair follicles in *Tpp1*$^{\Delta/\Delta}$*K5-Cre* mice (Bitgood and McMahon, 1995).

We addressed whether defective downgrowth and development of mature hair follicles in *Tpp1* null epidermis was accompanied by reduced proliferation specifically in the hair follicles. Proliferation was reduced specifically at the hair primordiums of P4 *Tpp1*$^{\Delta/\Delta}$*K5-Cre* epidermis compared to age-matched wild-type hair follicles, and this defect was not apparent in interfollicular epidermis of *Tpp1*$^{\Delta/\Delta}$*K5-Cre* mice (Figure 6J), indicating that hair bulge cells are more sensitive to persistent telomere damage induced by *Tpp1* deletion. We next addressed whether decreased hair follicle SC proliferation in *Tpp1*$^{\Delta/\Delta}$*K5-Cre* mice was a cell-autonomous effect by using ex vivo clonogenic assays (Experimental Procedures). The number and size of colonies in this assay are considered to reflect, respectively, the number of epidermal SC and their ability to proliferate in vitro (Barrandon and Green, 1987). *Tpp1*$^{\Delta/\Delta}$*K5-Cre* keratinocytes showed significantly decreased clonogenic capacity (Figure 6K), suggesting that the proliferation defect of TPP1-deficient SC cells is cell autonomous.

Together, these findings suggest that *Tpp1* deletion does not affect Wnt/β-catenin-dependent hair follicle specification but instead has a profound negative impact on hair follicle downgrowth, proliferation, and differentiation, affecting the establishment of a mature hair bulge SC compartment, which explains the observations that these mice do not grow hair and show severe skin dryness.

## p53 Deficiency Rescues Skin Hyperpigmentation and Hair Growth Defects in *Tpp1*$^{\Delta/\Delta}$*K5-Cre p53*$^{-/-}$ Mice

Analysis of *Tpp1*-deficient MEFs suggested that p53 is an important mediator of cell-cycle arrest produced by TPP1 abrogation (Figure S1). To address whether the same was true in vivo in the context of mouse epidermis, we first studied the expression of the p53 and p21 cell-cycle inhibitors in skin sections. *Tpp1*$^{\Delta/\Delta}$*K5-Cre* epidermis showed increased amounts of both cell-cycle inhibitors compared to controls (Figures 7A and 7B), indicating that *Tpp1* deletion in the context of the mouse epidermis leads to upregulation of the p53/p21 pathways.

(B) Representative images of metaphases of the indicated genotypes. Magnifications of the indicated aberrations are shown. Yellow arrowheads, sister telomere fusions; white arrowheads, MTS; red arrowheads, breaks/fragments.
(C) Chromosomal aberrations upon aphidicolin treatment. At least 30 metaphases from four wild-type and three *Tpp1*$^{\Delta/\Delta}$ independent MEFs were analyzed per condition. Error bars represent standard error. Magnifications of the indicated aberrations are shown.
(D) Immunofluorescence detection of PCNA-positive cells in wild-type and *Tpp1*$^{\Delta/\Delta}$ MEFs treated with Cre. The percentage of cells showing PCNA foci and PCNA pan-nuclear staining is shown. More than 150 cells from two independent MEFs per genotype were scored. Statistical comparisons use the Student's t test, and p values are indicated.
(E) Colocalization of TRF1-PCNA foci per cell in wild-type and *Tpp1*$^{\Delta/\Delta}$ MEFs treated with Cre. Statistical comparisons were done using the Student's t test, and p values are indicated.
(F) Representative images of PCNA (red) and TRF1 (green) staining and of colocalization events (yellow; indicated with arrowheads) in wild-type and *Tpp1*$^{\Delta/\Delta}$ MEFs treated with Cre.
(G) Quantification of BrdU-positive cells in the indicated genotypes in the absence of treatment (no IR) and after 30 Gy of ionizing radiation. At least 200 cells from two independent MEFs per genotype were analyzed per condition.
(H) Quantification of the number of BrdU foci that colocalize with TRF1 in two wild-type and two *Tpp1*-depleted independent MEFs. At least 80 nuclei were analyzed per genotype. Statistical significance was determined by Student's t test, and the p value is indicated.
(I) Representative images of BrdU (green) and TRF1 (red) fluorescence. BrdU-TRF1 colocalization events (yellow) are indicated with arrows.

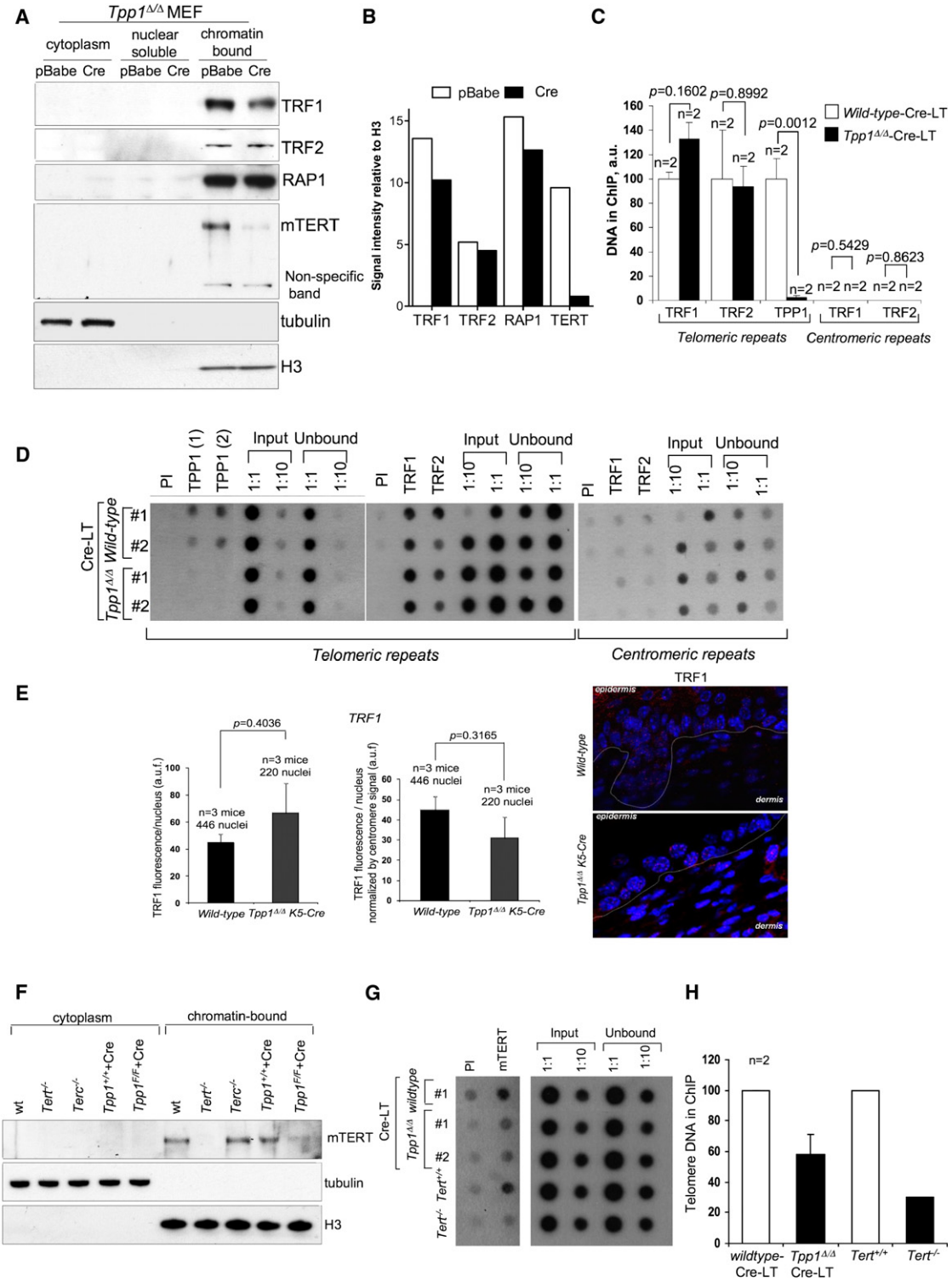


**Figure 4. TPP1 Recruits TERT to Telomeres in the Absence of Changes in TRF1 Levels**

(A) Subcellular fractionation of *Tpp1*$^{\Delta/\Delta}$-Cre-LT or control MEFs treated with pBabe vector. Note a decrease in mouse TERT (mTERT) bound to chromatin in *Tpp1*-depleted MEFs compared to control MEFs, whereas a nonspecific band produced by the TERT antibody did not change. Tubulin was used as a loading control for the cytoplasmic fraction and histone H3 for the chromatin-bound fraction.

(B) Quantification of different proteins relative to H3 levels is shown.

(C and D) ChIP of wild-type and *Tpp1*$^{\Delta/\Delta}$-Cre-LT MEFs using specific antibodies against TPP1, TRF1, and TRF2. Two different sera, indicated as 1 and 2, were used to immunoprecipitate TPP1. TRF1 and TRF2 immunoprecipitates were also probed with a mouse major satellite probe. The amount of immunoprecipitated

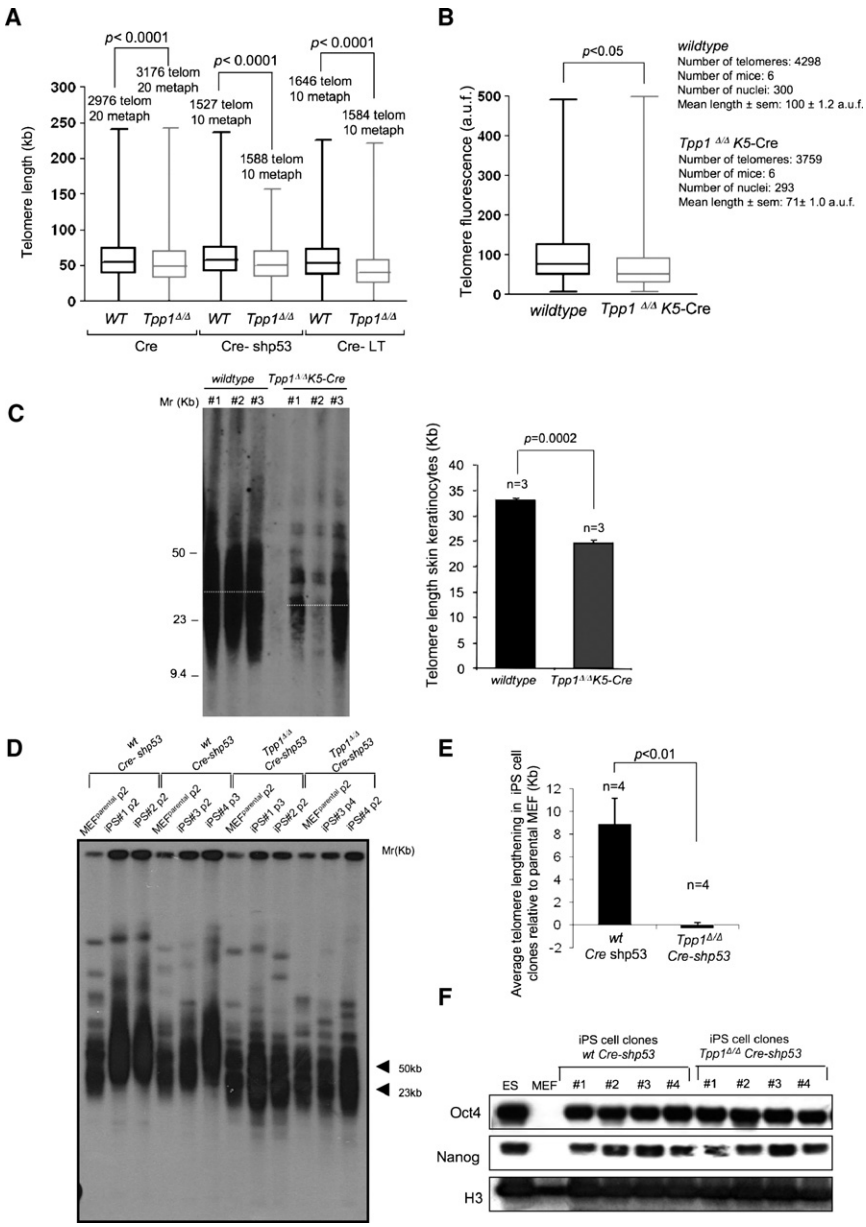


**Figure 5. TPP1 Is Required for Telomere Maintenance In Vivo and for Net Telomere Elongation during Nuclear Reprogramming**

(A) Telomere fluorescence (Q-FISH) distribution of individual telomere dots in metaphase spreads of MEFs from the indicated genotypes. The numbers of metaphases and telomeres used for the analysis are shown per genotype. The Student's t test was used for statistical calculations, and p values are indicated.

(B) Distribution of telomere fluorescence as determined by Q-FISH in skin sections from a total of six mice per genotype after correction by centromere fluorescence (not shown). The Student's t test was used for statistical calculations, and p values are indicated.

(C) Telomere shortening in skin keratinocytes from *Tpp1*$^{\Delta/\Delta}$*K5-Cre* newborn mice. Right: mean telomere length (kb) and standard error values are shown per genotype. n, independent mice used for the analysis. The Student's t test was used for statistical calculations, and p values are indicated. Left: representative TRF blot. The white dotted line indicates mean telomere length.

(D) TPP1 is required for net telomere elongation during nuclear reprogramming. Telomere restriction fragment (TRF) analysis in mouse *Tpp1*$^{+/+}$ and *Tpp1*$^{\Delta/\Delta}$ iPS cells at passage 2-3 after clone isolation, and their corresponding parental MEFs (passage 2). Two independent iPS clones derived from each MEF were analyzed. Note that telomeres are elongated in *Tpp1*$^{+/+}$ iPS cells compared to their corresponding parental MEF. This telomere elongation is, however, abolished in iPS cells derived from *Tpp1*$^{\Delta/\Delta}$ MEFs.

(E) Average lengthening of iPS clones when compared to their corresponding parental MEF, expressed in kb. Note that *Tpp1*$^{+/+}$ iPS clones show a net elongation of telomeres that is abolished in iPS cells derived from *Tpp1*$^{\Delta/\Delta}$ MEFs. n, total number of iPS clones analyzed. Statistical significance was determined by Student's t test.

(F) Robust expression of pluripotency markers Oct-4 and Nanog in iPS cells of the indicated genotypes.

To address the relevance of this increased p53 signaling, we generated *Tpp1*$^{\Delta/\Delta}$*K5-Cre p53*$^{-/-}$ mice. Notably, *Tpp1*$^{\Delta/\Delta}$*K5-Cre p53*$^{-/-}$ mice showed normal hair growth and no skin hyperpigmentation phenotype (Figure 7C), in agreement with recently published data with the *acd* mouse model as well as with our own observations with the *Trf1* null mouse model (Martinez et al., 2009). These results suggest an important role for p53 in restricting the establishment of the mature hair follicle stem

telomere or centromere repeats was normalized against the amount of telomere or centromere repeats present in the crosslinked chromatin fraction unbound to the preimmune serum, respectively. n, independent MEFs used. Bars represent the average between replicates; standard error is shown. Quantification of ChIP values for telomere and centromere repeats is shown in (C). A Student's t test was used to calculate statistical significance. Representative TPP1, TRF1, and TRF2 ChIPs with MEFs of the indicated genotypes are shown in (D).

(E) Average TRF1 fluorescence (a.u.f.) per nucleus in back skin sections from the indicated genotypes before or after correction by average centromere fluorescence (not shown). Error bars represent standard error. p values were calculated using the Student's t test. Representative images show TRF1 (red) fluorescence in the epidermis of the indicated genotypes. The dotted line delineates the epidermis-dermis boundary. Nuclei are counterstained with DAPI (blue).

(F) Subcellular fractionation of wild-type, *Tert*$^{-/-}$, *Terc*$^{-/-}$, and *Tpp1*$^{\Delta/\Delta}$-Cre-LT MEFs or control MEFs treated with pBabe vector (pBabe). Tubulin was used as a loading control for the cytoplasmic fraction and histone H3 for the chromatin-bound fraction.

(G and H) ChIP of wild-type and *Tpp1*$^{\Delta/\Delta}$-Cre-LT MEFs using specific antibodies against TERT. *Tert*$^{-/-}$ MEFs were used as a control for the specificity of the ChIP assay. The amount of immunoprecipitated telomere repeats was normalized against the amount of telomere repeats present in the crosslinked chromatin fraction unbound to the preimmune serum. Representative TERT ChIP with MEFs of the indicated genotypes is shown in (G). Quantification of ChIP values for telomere repeats is shown in (H).

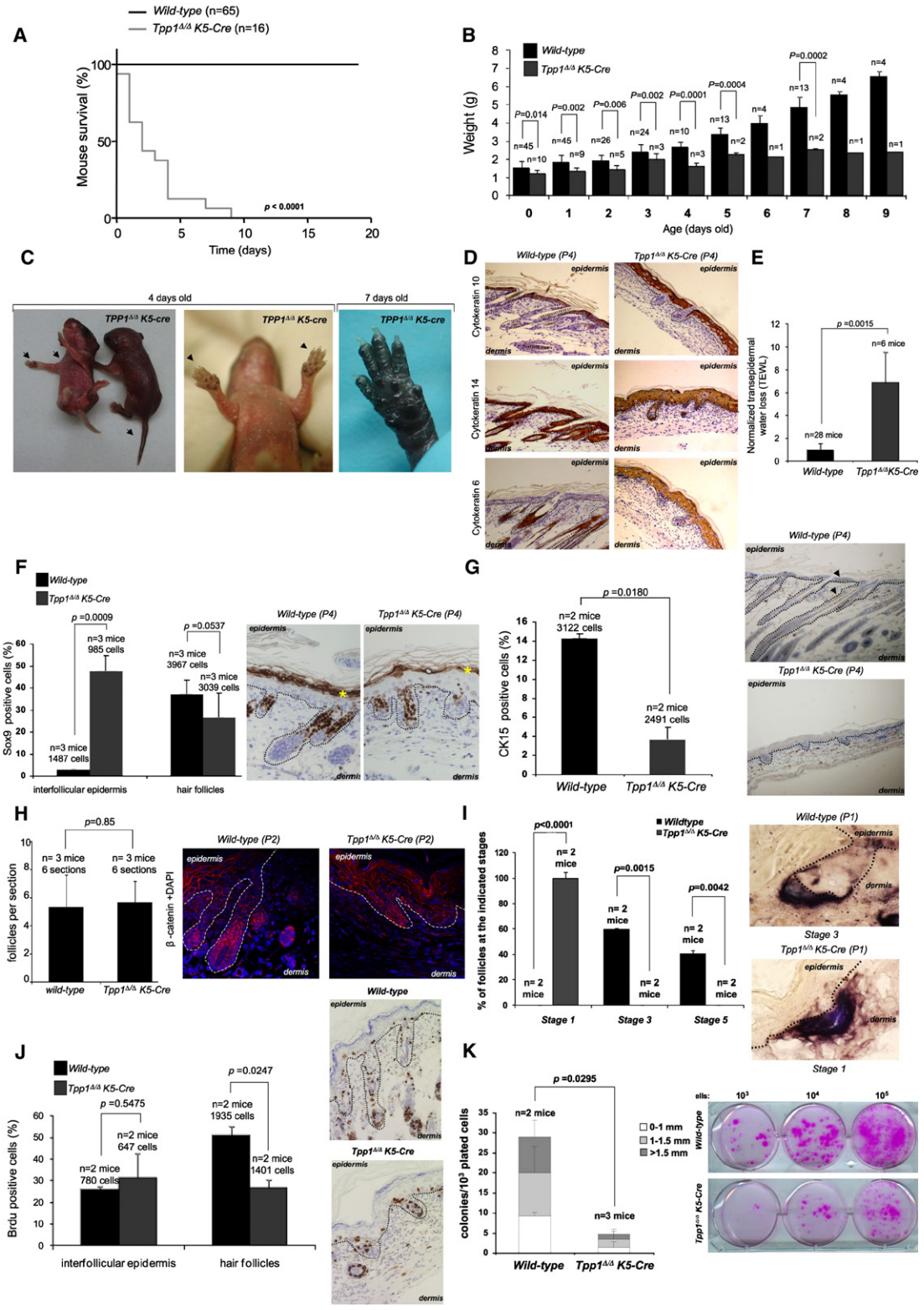


**Figure 6. *Tpp1* Deficiency Results in Perinatal Mortality and Severe Epithelial Abnormalities**

(A) Kaplan-Meier survival curve of wild-type and *Tpp1*$^{\Delta/\Delta}$*K5-Cre* mice. $\chi^2$ test was used to calculate statistical significance, and p values are indicated. n, mice included in the analysis.

(B) *Tpp1*$^{\Delta/\Delta}$*K5-Cre* mice are born with low body weight and do not gain weight in the following days compared to wild-type littermates. Student's t test was used for statistical calculations; standard errors and p values are shown. n, number of mice.

cell niche, as well as in restricting hair follicle downgrowth. In addition, p53 deficiency was able to significantly rescue both mouse survival and body weight (Figures 7D and 7E), and this effect was allele dose dependent as indicated by a significant rescue of these phenotypes in *Tpp1*$^{\Delta/\Delta}$*K5-Cre p53*$^{+/-}$ mice.

## DISCUSSION

Here we describe a mouse model for complete *Tpp1* abrogation. *Tpp1* abrogation leads to DDR activation at chromosome ends and increased telomere fusions and fragility, suggestive of a role for TPP1 in telomere protection. In addition, we demonstrate that TPP1 is required for TERT recruitment to telomeres and telomere elongation in vivo. In particular, TPP1 is essential for telomere elongation during nuclear reprogramming of MEFs into iPS cells, a process that involves net telomere elongation by telomerase (Marion et al., 2009a, 2009b). Interestingly, *TERT* and *Tpp1* show similar patterns of mRNA expression during embryonic development (Martin-Rivera et al., 1998; Vlangos et al., 2009), further suggesting their coregulation.

When deleted in the context of the mouse stratified epithelia, *Tpp1* deficiency leads to perinatal death, severe skin hyperpigmentation, defective hair follicle morphogenesis, and widespread epithelia dysplasia. These epithelial pathologies are similar to, although milder than, those produced by *TRF1* abrogation in the skin (Martinez et al., 2009), as well as to epithelial pathologies in human diseases associated with mutations in telomerase-related genes and the presence of dysfunctional telomeres (Armanios et al., 2007; Mitchell et al., 1999; Tsakiri et al., 2007; Vulliamy et al., 2001), making *Tpp1*-deleted mice a useful model for understanding human disease.

In this regard, we show here that hair follicle morphogenesis defects in *Tpp1* null skin are not associated with a defective Wnt/β-catenin pathway, a known regulator of hair follicle development in mice (Huelsken et al., 2001; Paus et al., 1999; Zhang et al., 2008), recently described to be regulated by TERT levels (Park et al., 2009). Instead, *Tpp1* abrogation had a profound negative impact on hair follicle downgrowth, proliferation, and differentiation, hindering the establishment of a mature hair bulge SC compartment. Importantly, these defects are rescued by p53 abrogation, supporting a key role of p53 in mediating proliferative arrest in response to persistent telomere damage in vivo (Chin et al., 1999; Feldser and Greider, 2007; Martinez et al., 2009; Stout and Blasco, 2009). Together, these findings indicate that TPP1 has a dual role in telomere protection and telomere elongation, in this way preserving telomere function and preventing the early onset of degenerative pathologies in mice.

## EXPERIMENTAL PROCEDURES

### Cell Fractionation and Immunoblotting

Cell fractionation was performed as described (Mendez and Stillman, 2000). Equal amounts of protein (50–100 mg) were analyzed by gel electrophoresis followed by western blotting. Anti-tubulin or anti-histone H3 antibodies were used as loading controls.

### Immunofluorescence In Situ Hybridization

Mitotic cells were prepared and subjected to immunofluorescence staining as described (Martinez et al., 2009).

### Retroviral Infections

Retroviral supernatants were produced in 293T cells ($5 \times 10^5$ cells per 100 mm diameter dish) transfected with the ecotropic packaging plasmid pCL-Eco and either pBabe-Cre, pRS-p53sh (Brummelkamp et al., 2002), or pZip-Neo-sv40-LT (Brown et al., 1986) as described (Martinez et al., 2009). Deletion of *Tpp1* was confirmed by PCR with primers Tpp1Up2 and Tpp1Lo2, and absence of TPP1 expression was tested by real-time quantitative RT-PCR and immunofluorescence.

### Transfection of Small Interference RNAs

HeLa 1.2.11 cells were transfected with the indicated siRNAs using Oligofectamine (Invitrogen Life Technologies) (Supplemental Information). A GFP siRNA was used as a control.

### *Tpp1* Knockdown Using Short Hairpin RNA Vectors

*Terc*$^{-/-}$ MEFs were infected with an shRNA effective in downregulating *mTpp1* expression (Supplemental Information). As a control, cells were transfected with a scrambled shRNA.

(C) Macroscopic phenotypes. Note that the skin of a 4-day-old *Tpp1*$^{\Delta/\Delta}$*K5-Cre* mouse shows a shiny appearance, scaling, and hyperpigmentation in the paws and tail (arrowheads, left and middle). Hyperpigmentation is aggravated in 7-day-old mice.
(D) Representative images of back skin sections stained for cytokeratin 10, cytokeratin 14, and cytokeratin 6. Note aberrant expression of cytokeratin 6 in *Tpp1*-depleted epidermis.
(E) Compromised epidermal barrier function in *Tpp1*$^{\Delta/\Delta}$*K5-Cre* mice. Transepidermal water loss (TEWL) normalized to wild-type levels (set to 1) is shown. n, mice analyzed per genotype. Error bars represent standard error. Student's t test was used for statistical analysis, and p values are indicated.
(F) Percentage of Sox9-positive cells at the interfollicular epidermis and at the hair follicles in back skin sections from mice of the indicated genotypes. n, mice analyzed per genotype. Right: representative images of Sox9-positive staining in the skin of 4-day-old mice. The dotted line separates dermis from epidermis. *, the staining in the top of the epidermis presumably represents background.
(G) Percentage of cytokeratin 15 (K15) -positive cells in back skin sections of mice of the indicated genotypes. n, mice analyzed per genotype. Right: representative images of K15-positive staining in the skin of 4-day-old mice.
(H) Similar number of follicles in back skin sections from P2 mice of the indicated genotypes. β-catenin expression was used to identify hair follicles. Error bars represent standard deviation. Statistical analysis was carried out using Student's t test, and p values are indicated. Right: representative images of immunofluorescence staining using a β-catenin antibody (red). Nuclei are counterstained with DAPI (blue).
(I) Average number of follicles at the indicated stages of development in both wild-type and *Tpp1*$^{\Delta/\Delta}$ *K5-Cre* tail skin sections. Error bars represent standard deviation. Statistical analysis was carried out with the $\chi^2$ test, and p values are indicated. Stages are quantified as described (Muller-Rover et al., 2001). Right: representative images of dermal papilla (blue/brown) localization in the indicated genotypes.
(J) Percentage of BrdU-positive cells in the interfollicular epidermis and in the hair follicles of back skin sections from mice of the indicated genotypes. n, mice analyzed per genotype. Right: representative images of BrdU-positive staining in the skin of 4-day-old mice. The dotted line separates dermis from epidermis.
(K) Quantification of size and number of epidermal SC clones obtained ex vivo. Right: representative examples of SC clones obtained from newborn mice (1-2 days old) at the indicated dilutions. Clones were visualized by rhodamine staining. n, mice analyzed per genotype. The total number of cells scored per genotype is indicated in each case. Error bars represent standard error. Student's t test was used for statistical analysis, and p values are shown.

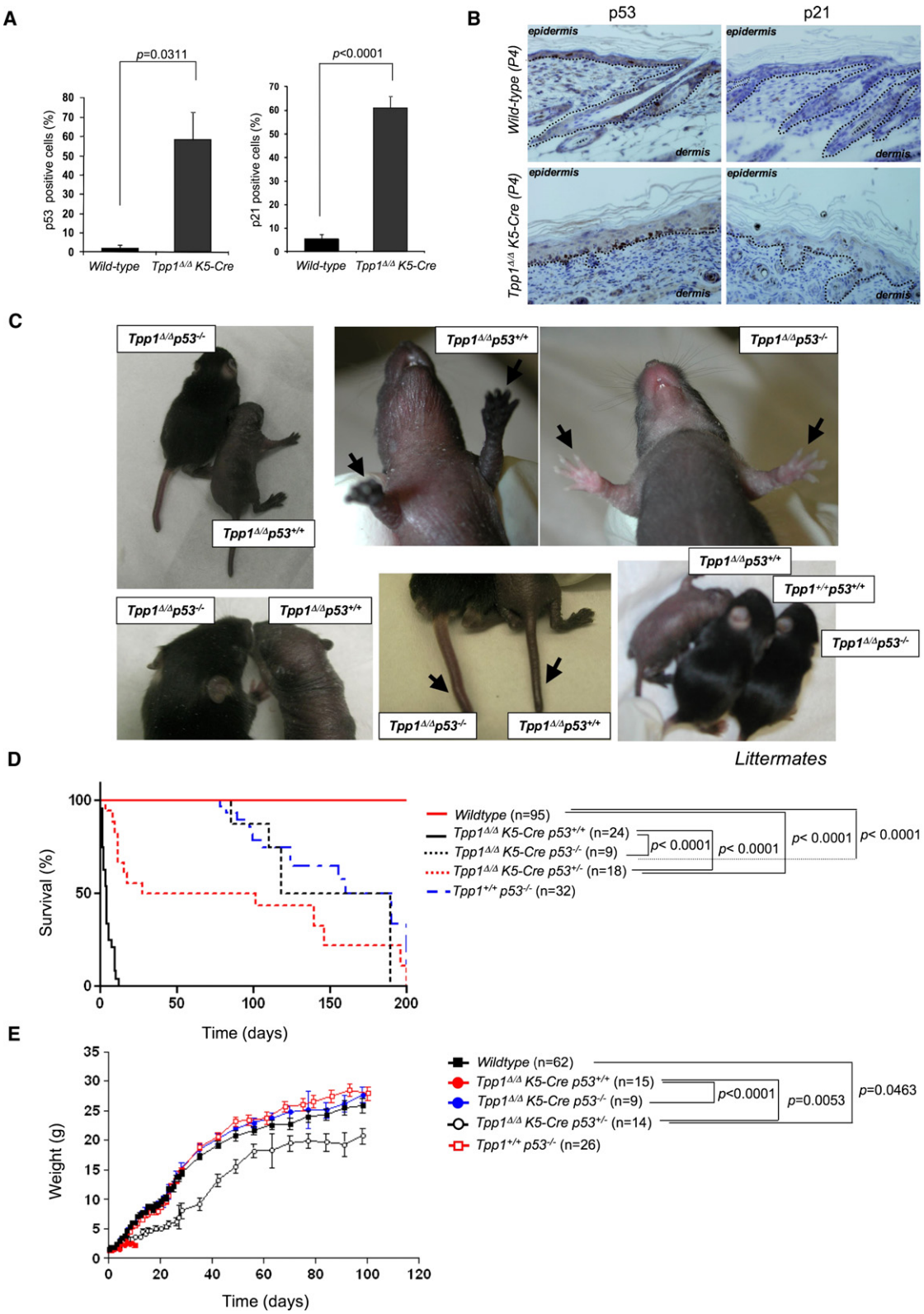


**Figure 7. p53 Mediates Proliferative Defects and Hyperpigmentation of *Tpp1*$^{\Delta/\Delta}$ *K5-Cre* Mice**

(A) Percentage of p53- and p21-positive cells in back skin sections from at least two mice per genotype. Error bars represent standard error. Student's t test was used for statistical analysis, and p values are indicated.

(B) Representative images of p53 and p21 staining in mouse back skin of the indicated genotypes. The dotted line separates epidermis from dermis.

### Generation of Mouse iPS Cells

*Tpp1*$^{+/+}$*-Cre* and *Tpp1*$^{\Delta/\Delta}$*-Cre* primary MEFs were obtained by retroviral infection with pBabe-Cre as described above. Puromycin-selected cells were then reprogrammed as previously described (Marion et al., 2009b). Briefly, MEFs were seeded and infected four times in the following 2 days with a cocktail of the retroviral constructs pMXsOct3/4, pMXsKlf4, pMXsSox2, and pRS-p53sh. Colonies were picked after 2 weeks and expanded on feeder fibroblasts using standard procedures. iPS cells were transferred to gelatin-coated plates before analysis.

### Real-Time Quantitative RT-PCR

Total RNA was extracted from the indicated cells using TRIzol (Invitrogen Life Technologies). Reverse transcription was carried out with 1 μg of total RNA using random hexamers as primers and Superscript II reverse transcriptase (Invitrogen Life Technologies) in accordance with the manufacturer's instructions. Real-time PCR was performed as described (Munoz et al., 2005). Primer sequences are shown in Supplemental Experimental Procedures.

### Telomere and Centromere Fluorescence Analyses of Skin Sections

Quantitative telomere and centromere fluorescence in situ hybridization (Q-FISH) on skin sections was performed as described (Munoz et al., 2005). For the centromeric Q-FISH, a probe against the major satellite was used (Flores et al., 2008).

### Telomere Length and Cytogenetic Analysis Using Telomere Q-FISH on Metaphases

Q-FISH on metaphases from primary MEFs was performed as described (Herrera et al., 1999; Samper et al., 2000). When indicated, MEFs were treated with aphidicolin at 0.5 μM for 24 hr. For analysis of chromosomal aberrations, quantitative analysis of digital images was performed as described in Zijlmans et al. (1997).

### TRF and G-Strand Overhang Analysis

Half a million keratinocytes, MEFs, or iPS cells were included in agarose plugs and TRF analysis was performed as described (Blasco et al., 1997).

The G-strand overhang assay was carried out as described (Samper et al., 2000). For quantitative analysis of telomere length in iPS cells, each lane was divided into 32 identical fractions covering the entire TRF smear. The weighted mean was calculated by measuring the signal intensity of each fraction, expressed as the percentage of the total signal intensity of the lane. The ImageJ program was used for quantification.

### Telomerase TRAP Assay

Telomerase activity was measured with a modified telomere repeat amplification protocol (TRAP) as described (Blasco et al., 1997).

### Chromatin Immunoprecipitation Assays

ChIP assays were performed as described (Garcia-Cao et al., 2004) with the following antibodies: 8 μl of rabbit anti-mouse TRF1 serum (generated in our lab), 4 μl of rabbit polyclonal anti-TRF2 antibody (a gift from Dr. West, CR-UK), 8 μl of two different rabbit anti-mouse TPP1 sera (a gift from Dr. Else, University of Michigan), and 6 μl of rabbit polyclonal anti-TERT antibody (Calbiochem) or preimmune serum. The amount of telomeric and pericentric DNA after ChIP was normalized to the total telomeric or centromeric signal, respectively, for each genotype, thus correcting for differences in the number of telomere repeats.

### Treatment with ATM and ATR Inhibitors

Wild-type and *Tpp1* null MEFs were treated with either 10 μM ATM-specific inhibitor KU55933 (Tocris Bioscience) or 5 μM caffeine (Sigma) and processed as described (Martinez et al., 2009).

### Proliferation Assays

*Tpp1*$^{flox/flox}$ cells (5 × 10$^4$) infected with Cre or Cre-shp53 were distributed into six-well plates at day 0. For direct cell counting, attached cells were trypsinized and counted using a Neubauer chamber slide at the indicated times.

### Isolation of Keratinocytes from Newborn Mice Skin and ESC Clonogenic Assays

Primary keratinocytes from newborn mice (0–2 days old) were obtained as described (Munoz et al., 2005) and clonogenic assays performed as described (Flores et al., 2005).

### Flow Cytometric Analysis

Keratinocytes (1 × 10$^6$) were washed twice with PBS and fixed/permeabilized with ice-cold 70% ethanol. Fixed cells were washed with PBS and resuspended in 1 ml PBS containing 0.2 μg propidium iodide and 100 μg RNase. The samples were incubated 30 min at 37°C and the fluorescence-activated cell sorting (FACS) analysis was performed in a FACSCanto II flow cytometry system (BD Biosciences). The data were analyzed with the software FACSDiva v5.1.1.

### Immunohistochemistry, Immunofluorescence, and Senescence-Specific β-Gal Staining Techniques

Immunohistochemistry was performed on deparaffinated skin sections processed with 10 mM sodium citrate (pH 6.5) cooked under pressure for 2 min. Slides were washed in water, then in Tris-buffered saline (TBS) with 0.5% Tween 20, blocked with peroxidase, washed with TBS with 0.5% Tween 20 again, and blocked with fetal bovine serum followed by another wash and then incubated with the indicated antibodies (Supplemental Information). For signal development, DAB (Dako) was used as a substrate. Sections were lightly counterstained with hematoxylin and analyzed by light microscopy.

For immunofluorescence analysis of paraffin sections, skin sections were permeabilized with 0.5% Triton X-100 buffer at room temperature for 45 min, and blocked with fetal bovine serum for 1 hr. For immunofluorescence of OCT sections, 8 μM cryosections were fixed in 4% paraformaldehyde-PBS for 10 min at room temperature, rinsed in PBS, and then permeabilized with Triton X-100 0.5% twice for 15 min each at room temperature. The sections were incubated overnight at 4°C with the indicated antibodies (Supplemental Information). Images were obtained using a fluorescence microscope (Leica DMRB). Quantitative image analysis of TRF1 was performed on images obtained using a confocal microscope (Leica TCS-SP5 DOBS).

For ssDNA and TRF1 immunofluorescence, cells were attached to coverslips and treated with BrdU (10 μM) for 48 hr. Cells were treated with 0 or 30 Gy of ionizing radiation and left for 90 min in PBS. Then, cells were fixed with ice-cold methanol for 1 hr at −20°C, blocked with PBS-Tween (0.1%) for 20 min at room temperature, and probed with the indicated antibodies (Supplemental Information), and slides were stained with DAPI and mounted in Vectashield.

For telomere PNA-53BP1 immuno-Q-FISH, 53BP1 immunofluorescence was carried out as described above and then the telomeric PNA probe was hybridized following the quantitative telomere fluorescence in situ hybridization (Q-FISH) protocol described below with the exception that 50% formamide was used in the washing steps.

Senescence was analyzed with the β-galactosidase staining kit (Cell Signaling) following the manufacturer's advice.

### Dermal Papilla Detection on Skin Sections

Neonate tail skin (1–4 days old) was embedded in OCT blocks. Cryosections (10 μM) were fixed in 4% paraformaldehyde-PBS for 10 min at room temperature and then rinsed in PBS. Excess PBS was removed and 50–75 μl of developing solution (100 mM Tris [pH 9.5], 100 mM NaCl, 50 mM $MgCl_2$), NBT (nitro

(C) p53 deficiency rescues proliferative defects and hyperpigmentation of *Tpp1*$^{\Delta/\Delta}$*K5-Cre* mice. *Tpp1*$^{\Delta/\Delta}$*K5-Cre p53*$^{-/-}$ mice develop hair and do not show skin hyperpigmentation. Arrows indicate hyperpigmentation or lack of it in paws and tail.
(D) Survival curve of wild-type, *Tpp1*$^{\Delta/\Delta}$*K5-Cre*, *Tpp1*$^{\Delta/\Delta}$*K5-Cre p53*$^{-/-}$, *Tpp1*$^{\Delta/\Delta}$*K5-Cre p53*$^{+/-}$, and *Tpp1*$^{+/+}$ *p53*$^{-/-}$ mice. $\chi^2$ test was used to calculate statistical significance, and p values are indicated. n, number of mice included in the analysis.
(E) p53 deficiency rescues the low body weight of *Tpp1*$^{\Delta/\Delta}$*K5-Cre* mice; *Tpp1*$^{\Delta/\Delta}$*K5-Cre p53*$^{-/-}$ body weight is similar to that of wild-type littermates. Student's t test was used for statistical calculations; standard error and p values are shown. n, number of mice.

blue tetrazolium chloride; Roche), and BCIP (5-bromo-4-chloro-3-indoxyl phosphate; Roche) were added. Samples were incubated for up to 10 min at room temperature, with the development of the reaction checked by microscope. The reaction was stopped by washing with distilled water twice for 30 s each. Sections were mounted with Vectashield. The number of follicles was counted per genotype and scored according to developmental stage as described (Muller-Rover et al., 2001) using an Olympus Provis AX70 light microscope.

### Transepidermal Water Loss

Transepidermal water loss (TEWL) was measured with a Tewameter TM 300 (CK Electronics).

### Histopathological Analyses

Skin samples and other mouse tissues were fixed in 10% buffered formalin, dehydrated, and embedded in paraffin. For histopathological analysis, 4 μm sections were deparaffinated and stained with hematoxylin and eosin according to standard procedures. Images were captured with a DP-10 digital camera under an Olympus Vanox microscope at the indicated magnifications. To study proliferation in epidermis, BrdU at a concentration of 50 mg/kg body weight in PBS was injected into newborn mice 4 hr prior to sacrifice.

### In Situ Hybridization for Detection of *Shh* mRNA Expression

Digoxigenin probe synthesis was performed according to the manufacturer's instructions (Roche). cRNA probes from a 2.8 kb mouse *Shh* cDNA in pBlueScript KS$^+$ were made by either XbaI linearization and T7 transcription (antisense) or HindIII linearization and T3 transcription (sense). In situ hybridizations on 15 μm frozen sections obtained from E17.5 mice were performed as described (Gat et al., 1998).

### Statistical Analysis

A Student's t test was used to calculate the statistical significance of the observed differences in the percentage of TPP1-positive cells, RT-PCR, body weight, γH2AX foci, 53BP1 foci, TERT expression, BrdU incorporation, PCNA expression, p53 expression, p21 expression, Sox9 expression, cytokeratine 15 expression, β-catenin expression, P-cadherin expression, TRF1 expression, ChIP assays, TEWL, clonogenicity assays, flow cytometric analysis, TRAP assay, telomere length, and G-strand overhang. A $\chi^2$ test was used to calculate statistical significance in survival, pathologies, body weight curves, chromosomal aberrations, and dermal papilla stages.

## SUPPLEMENTAL INFORMATION

Supplemental Information includes Supplemental Experimental Procedures, five figures, and one table and can be found with this article online at doi:10.1016/j.devcel.2010.03.011.

## ACKNOWLEDGMENTS

We thank L. Harrington for *Tert*-deficient MEFs and M. Perez-Moreno for advice and reagents. We thank R. Serrano for mouse care and the Comparative Pathology Unit at CNIO for technical assistance. P.M. is a Ramon y Cajal senior scientist. M.A.B.'s laboratory is funded by the Spanish Ministry of Innovation and Science, the Consolider-Ingenio 2010 Programme, the European Union, the European Reseach Council (ERC Advance Grants), and the Körber European Science Award to M.A.B. The work in M. Tarsounas's laboratory is funded by Cancer Research UK. Travel related to this project was funded by a Joint International Award to M. Tarsounas and M.A.B. from The Royal Society.

Received: July 3, 2009
Revised: February 2, 2010
Accepted: March 29, 2010
Published: May 17, 2010

## REFERENCES

Armanios, M.Y., Chen, J.J., Cogan, J.D., Alder, J.K., Ingersoll, R.G., Markin, C., Lawson, W.E., Xie, M., Vulto, I., Phillips, J.A., III., et al. (2007). Telomerase mutations in families with idiopathic pulmonary fibrosis. N. Engl. J. Med. *356*, 1317–1326.

Barrandon, Y., and Green, H. (1987). Three clonal types of keratinocyte with different capacities for multiplication. Proc. Natl. Acad. Sci. USA *84*, 2302–2306.

Bitgood, M.J., and McMahon, A.P. (1995). Hedgehog and Bmp genes are coexpressed at many diverse sites of cell-cell interaction in the mouse embryo. Dev. Biol. *172*, 126–138.

Blanco, R., Munoz, P., Flores, J.M., Klatt, P., and Blasco, M.A. (2007). Telomerase abrogation dramatically accelerates TRF2-induced epithelial carcinogenesis. Genes Dev. *21*, 206–220.

Blanpain, C., and Fuchs, E. (2009). Epidermal homeostasis: a balancing act of stem cells in the skin. Nat. Rev. Mol. Cell Biol. *10*, 207–217.

Blasco, M.A., Lee, H.W., Hande, M.P., Samper, E., Lansdorp, P.M., DePinho, R.A., and Greider, C.W. (1997). Telomere shortening and tumor formation by mouse cells lacking telomerase RNA. Cell *91*, 25–34.

Brown, M., McCormack, M., Zinn, K.G., Farrell, M.P., Bikel, I., and Livingston, D.M. (1986). A recombinant murine retrovirus for simian virus 40 large T cDNA transforms mouse fibroblasts to anchorage-independent growth. J. Virol. *60*, 290–293.

Brummelkamp, T.R., Bernards, R., and Agami, R. (2002). A system for stable expression of short interfering RNAs in mammalian cells. Science *296*, 550–553.

Celli, G.B., and de Lange, T. (2005). DNA processing is not required for ATM-mediated telomere damage response after TRF2 deletion. Nat. Cell Biol. *7*, 712–718.

Chin, L., Artandi, S.E., Shen, Q., Tam, A., Lee, S.L., Gottlieb, G.J., Greider, C.W., and DePinho, R.A. (1999). p53 deficiency rescues the adverse effects of telomere loss and cooperates with telomere dysfunction to accelerate carcinogenesis. Cell *97*, 527–538.

d'Adda di Fagagna, F., Reaper, P.M., Clay-Farrace, L., Fiegler, H., Carr, P., Von Zglinicki, T., Saretzki, G., Carter, N.P., and Jackson, S.P. (2003). A DNA damage checkpoint response in telomere-initiated senescence. Nature *426*, 194–198.

de Lange, T. (2005). Shelterin: the protein complex that shapes and safeguards human telomeres. Genes Dev. *19*, 2100–2110.

Durkin, S.G., and Glover, T.W. (2007). Chromosome fragile sites. Annu. Rev. Genet. *41*, 169–192.

Else, T., Theisen, B.K., Wu, Y., Hutz, J.E., Keegan, C.E., Hammer, G.D., and Ferguson, D.O. (2007). Tpp1/Acd maintains genomic stability through a complex role in telomere protection. Chromosome Res. *15*, 1001–1013.

Else, T., Trovato, A., Kim, A.C., Wu, Y., Ferguson, D.O., Kuick, R.D., Lucas, P.C., and Hammer, G.D. (2009). Genetic p53 deficiency partially rescues the adrenocortical dysplasia phenotype at the expense of increased tumorigenesis. Cancer Cell *15*, 465–476.

Feldser, D.M., and Greider, C.W. (2007). Short telomeres limit tumor progression in vivo by inducing senescence. Cancer Cell *11*, 461–469.

Flores, I., Cayuela, M.L., and Blasco, M.A. (2005). Effects of telomerase and telomere length on epidermal stem cell behavior. Science *309*, 1253–1256.

Flores, I., Canela, A., Vera, E., Tejera, A., Cotsarelis, G., and Blasco, M.A. (2008). The longest telomeres: a general signature of adult stem cell compartments. Genes Dev. *22*, 654–667.

Garcia-Cao, M., O'Sullivan, R., Peters, A.H., Jenuwein, T., and Blasco, M.A. (2004). Epigenetic regulation of telomere length in mammalian cells by the Suv39h1 and Suv39h2 histone methyltransferases. Nat. Genet. *36*, 94–99.

Gat, U., DasGupta, R., Degenstein, L., and Fuchs, E. (1998). De novo hair follicle morphogenesis and hair tumors in mice expressing a truncated β-catenin in skin. Cell *95*, 605–614.

Herrera, E., Samper, E., Martin-Caballero, J., Flores, J.M., Lee, H.W., and Blasco, M.A. (1999). Disease states associated with telomerase deficiency appear earlier in mice with short telomeres. EMBO J. *18*, 2950–2960.

Hickson, I., Zhao, Y., Richardson, C.J., Green, S.J., Martin, N.M., Orr, A.I., Reaper, P.M., Jackson, S.P., Curtin, N.J., and Smith, G.C. (2004). Identification and characterization of a novel and specific inhibitor of the ataxia-telangiectasia mutated kinase ATM. Cancer Res. *64*, 9152–9159.

Hockemeyer, D., Daniels, J.P., Takai, H., and de Lange, T. (2006). Recent expansion of the telomeric complex in rodents: two distinct POT1 proteins protect mouse telomeres. Cell *126*, 63–77.

Hockemeyer, D., Palm, W., Else, T., Daniels, J.P., Takai, K.K., Ye, J.Z., Keegan, C.E., de Lange, T., and Hammer, G.D. (2007). Telomere protection by mammalian Pot1 requires interaction with Tpp1. Nat. Struct. Mol. Biol. *14*, 754–761.

Huelsken, J., Vogel, R., Erdmann, B., Cotsarelis, G., and Birchmeier, W. (2001). β-catenin controls hair follicle morphogenesis and stem cell differentiation in the skin. Cell *105*, 533–545.

Kaufman, C.K., Zhou, P., Pasolli, H.A., Rendl, M., Bolotin, D., Lim, K.C., Dai, X., Alegre, M.L., and Fuchs, E. (2003). GATA-3: an unexpected regulator of cell lineage determination in skin. Genes Dev. *17*, 2108–2122.

Keegan, C.E., Hutz, J.E., Else, T., Adamska, M., Shah, S.P., Kent, A.E., Howes, J.M., Beamer, W.G., and Hammer, G.D. (2005). Urogenital and caudal dysgenesis in adrenocortical dysplasia (acd) mice is caused by a splicing mutation in a novel telomeric regulator. Hum. Mol. Genet. *14*, 113–123.

Liu, Y., Snow, B.E., Hande, M.P., Yeung, D., Erdmann, N.J., Wakeham, A., Itie, A., Siderovski, D.P., Lansdorp, P.M., Robinson, M.O., and Harrington, L. (2000). The telomerase reverse transcriptase is limiting and necessary for telomerase function in vivo. Curr. Biol. *10*, 1459–1462.

Liu, Y., Lyle, S., Yang, Z., and Cotsarelis, G. (2003). Keratin 15 promoter targets putative epithelial stem cells in the hair follicle bulge. J. Invest. Dermatol. *121*, 963–968.

Liu, D., O'Connor, M.S., Qin, J., and Songyang, Z. (2004). Telosome, a mammalian telomere-associated complex formed by multiple telomeric proteins. J. Biol. Chem. *279*, 51338–51342.

Marion, R.M., Strati, K., Li, H., Murga, M., Blanco, R., Ortega, S., Fernandez-Capetillo, O., Serrano, M., and Blasco, M.A. (2009a). A p53-mediated DNA damage response limits reprogramming to ensure iPS cell genomic integrity. Nature *460*, 1149–1153.

Marion, R.M., Strati, K., Li, H., Tejera, A., Schoeftner, S., Ortega, S., Serrano, M., and Blasco, M.A. (2009b). Telomeres acquire embryonic stem cell characteristics in induced pluripotent stem cells. Cell Stem Cell *4*, 141–154.

Martin-Rivera, L., Herrera, E., Albar, J.P., and Blasco, M.A. (1998). Expression of mouse telomerase catalytic subunit in embryos and adult tissues. Proc. Natl. Acad. Sci. USA *95*, 10471–10476.

Martinez, P., Thanasoula, M., Munoz, P., Liao, C., Tejera, A., McNees, C., Flores, J.M., Fernandez-Capetillo, O., Tarsounas, M., and Blasco, M.A. (2009). Increased telomere fragility and fusions resulting from TRF1 deficiency lead to degenerative pathologies and increased cancer in mice. Genes Dev. *23*, 2060–2075.

McGavin, M.D., and Zachary, J.F. (2007). Pathologic Basis of Veterinary Disease, Fourth Edition (St. Louis: Mosby Elsevier).

Mendez, J., and Stillman, B. (2000). Chromatin association of human origin recognition complex, Cdc6, and minichromosome maintenance proteins during the cell cycle: assembly of prereplication complexes in late mitosis. Mol. Cell. Biol. *20*, 8602–8612.

Mitchell, J.R., Wood, E., and Collins, K. (1999). A telomerase component is defective in the human disease dyskeratosis congenita. Nature *402*, 551–555.

Miyoshi, T., Kanoh, J., Saito, M., and Ishikawa, F. (2008). Fission yeast Pot1-Tpp1 protects telomeres and regulates telomere length. Science *320*, 1341–1344.

Muller-Rover, S., Handjiski, B., van der Veen, C., Eichmuller, S., Foitzik, K., McKay, I.A., Stenn, K.S., and Paus, R. (2001). A comprehensive guide for the accurate classification of murine hair follicles in distinct hair cycle stages. J. Invest. Dermatol. *117*, 3–15.

Munoz, P., Blanco, R., Flores, J.M., and Blasco, M.A. (2005). XPF nuclease-dependent telomere loss and increased DNA damage in mice overexpressing TRF2 result in premature aging and cancer. Nat. Genet. *37*, 1063–1071.

Nowak, J.A., Polak, L., Pasolli, H.A., and Fuchs, E. (2008). Hair follicle stem cells are specified and function in early skin morphogenesis. Cell Stem Cell *3*, 33–43.

Park, J.I., Venteicher, A.S., Hong, J.Y., Choi, J., Jun, S., Shkreli, M., Chang, W., Meng, Z., Cheung, P., Ji, H., et al. (2009). Telomerase modulates Wnt signalling by association with target gene chromatin. Nature *460*, 66–72.

Paus, R., Muller-Rover, S., Van Der Veen, C., Maurer, M., Eichmuller, S., Ling, G., Hofmann, U., Foitzik, K., Mecklenburg, L., and Handjiski, B. (1999). A comprehensive guide for the recognition and classification of distinct stages of hair follicle morphogenesis. J. Invest. Dermatol. *113*, 523–532.

Ramirez, A., Bravo, A., Jorcano, J.L., and Vidal, M. (1994). Sequences 5′ of the bovine keratin 5 gene direct tissue- and cell-type-specific expression of a lacZ gene in the adult and during development. Differentiation *58*, 53–64.

Samper, E., Goytisolo, F.A., Slijepcevic, P., van Buul, P.P., and Blasco, M.A. (2000). Mammalian Ku86 protein prevents telomeric fusions independently of the length of TTAGGG repeats and the G-strand overhang. EMBO Rep. *1*, 244–252.

Sfeir, A., Kosiyatrakul, S.T., Hockemeyer, D., MacRae, S.L., Karlseder, J., Schildkraut, C.L., and de Lange, T. (2009). Mammalian telomeres resemble fragile sites and require TRF1 for efficient replication. Cell *138*, 90–103.

Silver, D.P., and Livingston, D.M. (2001). Self-excising retroviral vectors encoding the Cre recombinase overcome Cre-mediated cellular toxicity. Mol. Cell *8*, 233–243.

St-Jacques, B., Dassule, H.R., Karavanova, I., Botchkarev, V.A., Li, J., Danielian, P.S., McMahon, J.A., Lewis, P.M., Paus, R., and McMahon, A.P. (1998). Sonic hedgehog signaling is essential for hair development. Curr. Biol. *8*, 1058–1068.

Stoler, A., Duvic, M., and Fuchs, E. (1989). Unusual patterns of keratin expression in the overlying epidermis of patients with dermatofibromas: biochemical alterations in the epidermis as a consequence of dermal tumors. J. Invest. Dermatol. *93*, 728–738.

Stout, G.J., and Blasco, M.A. (2009). Genetic dissection of the mechanisms underlying telomere-associated diseases: impact of the TRF2 telomeric protein on mouse epidermal stem cells. Dis. Model. Mech. *2*, 139–156.

Takahashi, K., and Yamanaka, S. (2006). Induction of pluripotent stem cells from mouse embryonic and adult fibroblast cultures by defined factors. Cell *126*, 663–676.

Takai, H., Smogorzewska, A., and de Lange, T. (2003). DNA damage foci at dysfunctional telomeres. Curr. Biol. *13*, 1549–1556.

Tsakiri, K.D., Cronkhite, J.T., Kuan, P.J., Xing, C., Raghu, G., Weissler, J.C., Rosenblatt, R.L., Shay, J.W., and Garcia, C.K. (2007). Adult-onset pulmonary fibrosis caused by mutations in telomerase. Proc. Natl. Acad. Sci. USA *104*, 7552–7557.

Vidal, V.P., Chaboissier, M.C., Lutzkendorf, S., Cotsarelis, G., Mill, P., Hui, C.C., Ortonne, N., Ortonne, J.P., and Schedl, A. (2005). Sox9 is essential for outer root sheath differentiation and the formation of the hair stem cell compartment. Curr. Biol. *15*, 1340–1351.

Vlangos, C.N., O'Connor, B.C., Morley, M.J., Krause, A.S., Osawa, G.A., and Keegan, C.E. (2009). Caudal regression in adrenocortical dysplasia (acd) mice is caused by telomere dysfunction with subsequent p53-dependent apoptosis. Dev. Biol. *334*, 418–428.

Vulliamy, T., Marrone, A., Goldman, F., Dearlove, A., Bessler, M., Mason, P.J., and Dokal, I. (2001). The RNA component of telomerase is mutated in autosomal dominant dyskeratosis congenita. Nature *413*, 432–435.

Wu, L., Multani, A.S., He, H., Cosme-Blanco, W., Deng, Y., Deng, J.M., Bachilo, O., Pathak, S., Tahara, H., Bailey, S.M., et al. (2006). Pot1 deficiency initiates DNA damage checkpoint activation and aberrant homologous recombination at telomeres. Cell *126*, 49–62.

Xin, H., Liu, D., Wan, M., Safari, A., Kim, H., Sun, W., O'Connor, M.S., and Songyang, Z. (2007). TPP1 is a homologue of ciliate TEBP-β and interacts with POT1 to recruit telomerase. Nature *445*, 559–562.

Zhang, Y., Andl, T., Yang, S.H., Teta, M., Liu, F., Seykora, J.T., Tobias, J.W., Piccolo, S., Schmidt-Ullrich, R., Nagy, A., et al. (2008). Activation of β-catenin signaling programs embryonic epidermis to hair follicle fate. Development *135*, 2161–2172.

Zijlmans, J.M., Martens, U.M., Poon, S.S., Raap, A.K., Tanke, H.J., Ward, R.K., and Lansdorp, P.M. (1997). Telomeres in the mouse have large inter-chromosomal variations in the number of $T_2AG_3$ repeats. Proc. Natl. Acad. Sci. USA *94*, 7423–7428.